

www.acsnano.org

Piezoelectric Modulation of Excitonic Properties in Monolayer WSe₂ under Strong Dielectric Screening

Kanak Datta, Zidong Li, Zhengyang Lyu, and Parag B. Deotare*



Cite This: https://doi.org/10.1021/acsnano.1c04269



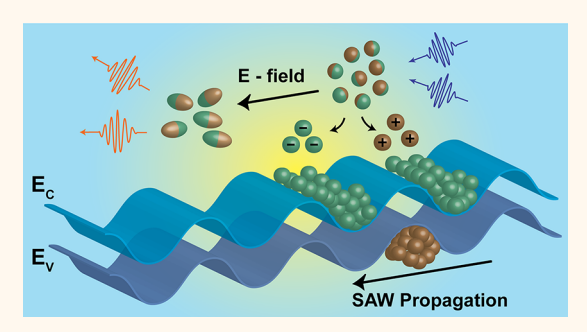
ACCESS

III Metrics & More

Article Recommendations

s Supporting Information

ABSTRACT: We investigate the interaction of excitons in monolayer WSe₂ with the piezoelectric field of surface acoustic wave (SAW) at room temperature using photoluminescence (PL) spectroscopy and report a large in-plane exciton polarizability of $8.43 \pm 0.18 \times 10^{-6}$ Dm/V. Such large polarizability arises due to the strong dielectric screening from the piezoelectric substrate. In addition, we show that the exciton-piezoelectric field interaction and population distribution between neutral excitons and trions can be optically manipulated by controlling the field screening using photogenerated free carriers. Finally, we model the broadening of the exciton PL line width and report that the interaction is dominated by type-II band edge modulation, because of the in-plane



electric field in the system. The results help understand the interaction of excitons in monolayer transition-metal dichalcogenides that will aid in controlled manipulation of excitonic properties for applications in sensing, detection, and on-chip communication.

KEYWORDS: surface acoustic wave, transition metal dichalcogenides, exciton polarizability, stark effect, exciton ionization, tungsten diselenide, type-II band edge modulation

INTRODUCTION

In recent years, semiconducting transition-metal dichalcogenide (TMD) monolayers have garnered widespread interest and persistent investigation from research communities across the world.^{1,2} The optical properties of these materials are dominated by excitons: Coulomb-bound electron-hole pairs that are known for very large oscillator strength.³ The strong quantum confinement and reduced dielectric screening results in large excitonic binding energy⁴⁻⁶ that enables manipulation of the excitonic response, even at room temperature using an external electric field or strain. Surface acoustic waves (SAWs) on a piezoelectric substrate provide a universal platform to simultaneously study the effect of both manipulation approaches. While SAW devices have been widely used in wireless radio frequency (RF) communication, they have been profoundly influential in advancing fundamental research.⁵ For instance, SAWs have been used as an effective tool for spatial and temporal manipulation of excitonic properties^{7,8} in embedded semiconducting nanostructures such as quantum well, quantum wire, quantum dot, and, more recently, monolayer two-dimensional materials such as $MoS_2^{15,16}$ and hexagonal boron nitride (h-BN). SAWs have also been used to realize high performing optoelectronic devices that operate on the principles of piezoelectric

dissociation ^{18,19} and to study charge transport in low-dimensional materials. ^{20–24} More importantly, SAW devices can generate large in-plane piezoelectric fields, which aligns with the large polarizability in TMDs, ^{25–27} compared to few orders of magnitude lower out-of-plane polarizability. ^{28–30}

In this work, we report the interaction of excitons in monolayer WSe_2 with SAW generated using lithium niobate (LiNbO₃) as the piezoelectric material at room temperature. The interaction of SAW with excitons in semiconducting nanostructures strongly depends on the type of band edge modulation in the semiconducting medium. In type-I band edge modulation, the spatial modulation of the conduction and valence bands with opposite phases creates periodic spatiotemporal traps³¹ that act as an efficient conveyor for excitons.³² On the other hand, in type-II modulation, strong built-in electric fields generated by the same spatial phase

Received: May 20, 2021 Accepted: June 22, 2021



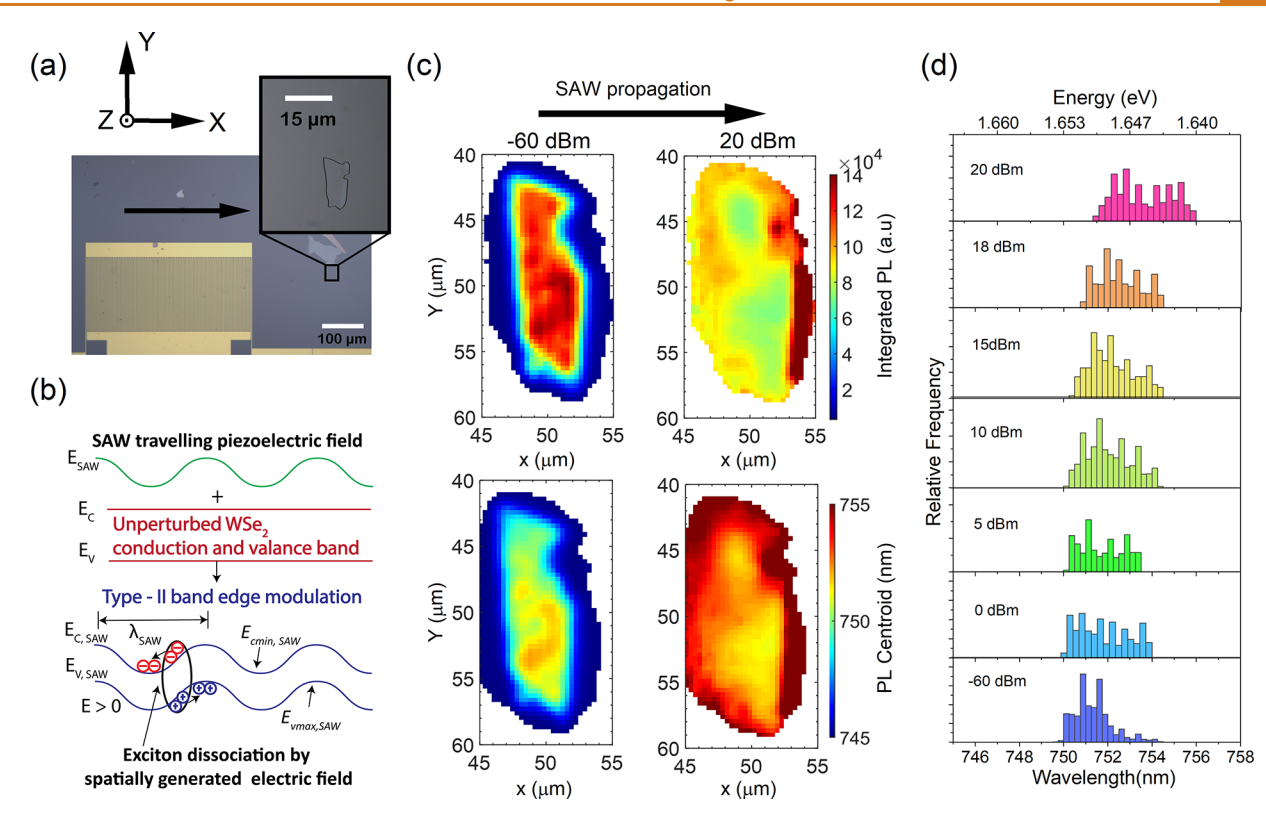


Figure 1. Exciton dissociation under surface acoustic wave in monolayer WSe₂. (a) Transferred monolayer WSe₂ (marked by black lines) on the delay line of the SAW device. The arrow in the figure shows the propagation direction of the acoustic wave. (b) A schematic representation of SAW induced exciton dissociation by type – II band edge modulation. Dissociated electrons and holes are accumulated at the conduction band minima ($E_{cmin, SAW}$) and valence band maxima ($E_{cmax, SAW}$) respectively. (c) Integrated PL intensity and PL centroid map of the monolayer WSe₂ at –60 dBm and 20 dBm RF input power levels (6 μ W optical excitation power). The SAW propagation direction is shown by the arrow on top. Strong PL quenching is observed as the SAW power is increased due to dissociation of excitons and trions into free carriers by the in-plane electric field. The centroid map shows stark effect induced redshift under SAW excitation. (d) Histogram of the PL centroid extracted from the PL map in (c). The centroid distribution in the histogram shows a gradual redshift as the RF input power is increased.

modulation of conduction and valence bands results in exciton dissociation into electron-hole pairs trapped at the piezoelectric potential pockets.³³ Under the latter scheme, the dissociated charges may be transferred and later recombined at a remote location as the electric field due to SAWs is screened/ removed by external means.³³ In our experiment, we observed the dominance of type-II modulation using high-frequency Rayleigh SAW waves³⁴ that were generated on a 128° Y-cut LiNbO₃ substrate using interdigitated transducers (IDTs) with a period (λ_{SAW}) of 6 μ m). The finger width of the IDTs was kept at half the IDT period and the acoustic aperture (the IDT finger overlap length) was >30 λ (acoustic measurements of the SAW transducers are shown in Section 1 in the Supporting Information). The mechanically exfoliated WSe₂ monolayer was transferred on the delay line of the SAW device. We observed that the high dielectric constant of the piezoelectric substrate contributed to the increased dielectric screening⁵ of the coulomb interaction between bound electron-hole pairs in the monolayer, reducing the exciton binding energy. Probing the monolayer photoluminescence (PL), we observed dissociation of excitons and trions under RF excitation along with a gradual shift of the overall distribution toward trion. The dissociation was accompanied by a strong Stark shift of the PL spectrum by the in-plane electric field of the SAW and PL line width broadening due to exciton ionization under the piezoelectric field. The observed dissociation, spectral shift, and broadening of the PL were strongly dependent on the

optically generated free-carrier screening in the monolayer. Based on the results, we estimated the in-plane polarizability of neutral excitons to be $8.43 \pm 0.18 \times 10^{-6}$ Dm/V, which agrees well with the theoretically predicted values. Such controlled manipulation of different excitonic species under external stimulus in a dielectrically screened environment can prove useful for next-generation excitonic devices serving applications from sensing, detection to on-chip communication, as well as integration of TMDs to substrates beyond silicon.

RESULTS AND DISCUSSION

Piezoelectric Dissociation of Excitons and Trions in Monolayer WSe₂ and Its Dependence on Optically Generated Free-Carrier Screening. A bright-field image of a mechanically exfoliated monolayer WSe₂ transferred along the SAW delay line is shown in Figure 1a, where the arrow marks the propagation direction of the acoustic wave. Under increased RF input power, the native band structure of the material is modified by the SAW's piezoelectric field (type-II band edge modulation dominates, because of the close proximity of the monolayer to the piezoelectric material) that results in potential pockets, which are spatially separated by half of the acoustic wavelength $(\lambda_{\text{SAW}}/2)$.³³ A simple schematic representation of such modulation is depicted in Figure 1b. The strong piezoelectric field dissociates the optically generated excitons and confines the electrons and

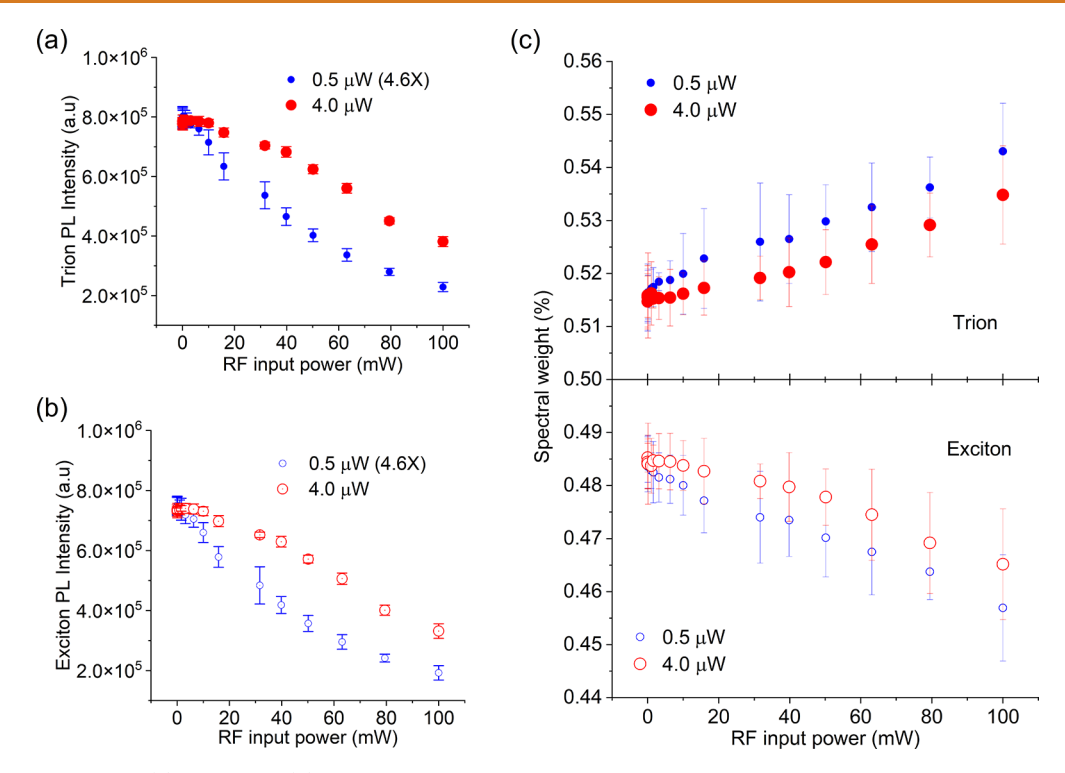


Figure 2. Effect of SAW on (a) trion and (b) exciton PL intensity with RF power at different optical excitations. To improve clarity of presentation, the exciton and trion PL intensities at $0.5 \,\mu\text{W}$ have been multiplied by a factor of 4.6. Accumulation of dissociated free carriers results in screening that leads to a decrease in the steady-state exciton and trion dissociation. The screening effect increases with optical excitation power. (c) Change in the exciton and trion spectral weight by the SAW electric field. An increase in the trion spectral weight and decrease in exciton spectral weight is observed with increased RF excitation input. The total range of spectral weight change varies with optical excitation, which confirm screened piezoelectric field in the monolayer at high optical excitations.

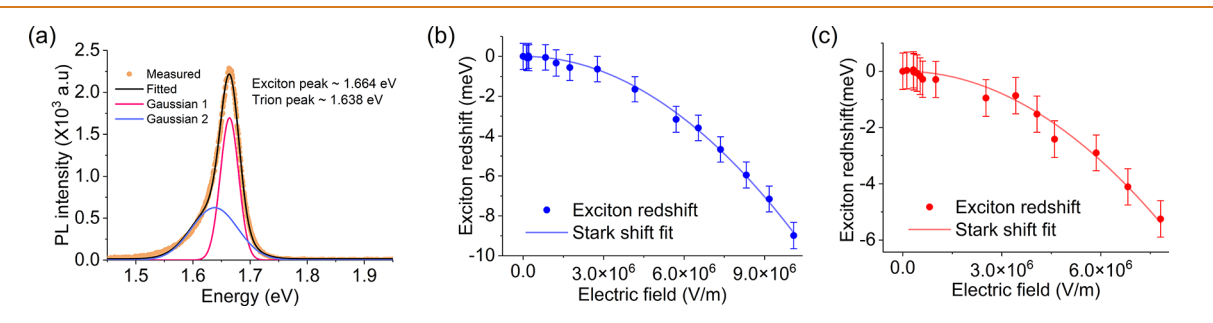


Figure 3. Spectral modulation of monolayer WSe₂ excitons under SAW electric field. (a) Two Gaussian fit of measured monolayer PL spectra at an optical input power of $0.5 \,\mu\text{W}$ and $-60 \,\text{dBm}$ input RF excitation. Fit to the excitonic redshift at (b) $0.5 \,\mu\text{W}$ average optical power using the quadratic stark shift equation that yield the in-plane neutral exciton polarizability of $8.36 \times 10^{-6} \,\text{Dm/V}$ and (c) $4 \,\mu\text{W}$ average optical power that yields a neutral exciton polarizability of $8.49 \times 10^{-6} \,\text{Dm/V}$. The error bars in panels (b) and (c) corresponds to the spread of PL measurements at different location on the monolayer sample. The quadrature dependence of the exciton spectral shift with the screened electric field confirms that the observed spectral shift is induced by the piezoelectric SAW field.

holes in the lateral potential pockets (conduction band minima $(E_{\rm cmin,SAW})$) and valence band maxima $(E_{\rm vmax,SAW})$). Figure 1c shows the PL intensity (at an optical power of 6 μ W) and centroid maps of the monolayer at RF input power levels of $-60~{\rm dBm}$ (the minimum RF power used in this work) and 20 dBm. The observed uniform spatial quenching of the integrated PL intensity with SAW confirms type-II band edge modulation by the traveling piezoelectric field, as reported previously in Group III–V semiconducting nanowires. The PL quenching is accompanied by a redshift of the monolayer's PL centroid, as evident from the centroid histogram for various RF input power, as shown in Figure 1d. The redshift is attributed to the stark shift by the in-plane component (in the direction of propagation) of the

propagating electric field of the SAW,²⁷ which is discussed later in the manuscript.

The effect of SAW piezoelectric potential on the dissociation of trions and excitons can be analyzed separately by extracting the integrated intensity of trions ($\int_{\lambda} I_{\text{PL,tr}}(\lambda) \; \mathrm{d}\lambda$) and excitons ($\int_{\lambda} I_{\text{PL,ex}}(\lambda) \; \mathrm{d}\lambda$) at different RF input power levels, as shown in Figures 2a and 2b, respectively. Here, $I_{\text{PL,ex}}(\lambda)$, $I_{\text{PL,tr}}(\lambda)$ refer to the estimated PL spectrum for the excitons and trions. These are extracted by fitting the spectra using two Gaussian functions corresponding to neutral A-excitons and trions, respectively $^{39-44}$ (We show two Gaussian fittings of a representative PL spectrum at an optical power of 0.5 μW at -60 dBm RF excitation in Figure 3a. The neutral A-exciton

and trion Gaussian peaks are located at ~1.664 and 1.638 eV, respectively. Refer to Section 3 in the Supporting Information for fitting of the corresponding PL spectra at 20 dBm RF excitation under the same optical input power. Consistent with the dissociation model due to piezoelectric field, we observe a gradual reduction in the neutral and charged exciton PL with an increase in the RF power. The corresponding PL spectra can be found in Section 6 in the Supporting Information. For a given RF level, the dissociation is reduced for higher optical incident powers (refer to Section 7 in the Supporting Information). This is because the SAW piezoelectric field is screened by the optically generated free carriers, thereby reducing the effective electric field that contributes to PL quenching. As a result, higher electric field is required to achieve the same level of PL quenching. We observed no spectral shift or broadening in the monolayer PL for a range of optical incident power between 0.5 μ W and 6 μ W (estimated exciton densities in the range of $1.4 \times 10^{10}/\text{cm}^2$ to $1.7 \times 10^{11}/$ cm;² refer to Section 2 in the Supporting Information) at very low RF input power levels of -60 dBm (refer to Section 4 in the Supporting Information). Hence, we rule out the contributions from optically induced heating and/or possible scattering with free carriers at higher excitation power. In addition, the integrated PL intensity of the exciton and trion peaks showed no signature of excitation-dependent nonlinearity (Section 5 in the Supporting Information).⁴⁵ Further analyses are thereby limited to the linear response regime.

We investigated the effect on the steady-state equilibrium between the excitonic species in the monolayer by extracting the spectral weight of trion, $\eta_{\text{PL,tr}} = \frac{\int_{\lambda} I_{\text{PL,tr}}(\lambda) \; \mathrm{d}\lambda}{\int_{\lambda} I_{\text{PL}}(\lambda) \; \mathrm{d}\lambda}$ and exciton,

$$\eta_{\mathrm{PL,ex}} = \frac{\int_{\lambda} I_{\mathrm{PL,ex}}(\lambda) \, \mathrm{d}\lambda}{\int_{\lambda} I_{\mathrm{PL}}(\lambda) \, \mathrm{d}\lambda}, \text{ where } \int_{\lambda} I_{\mathrm{PL}}(\lambda) \, \mathrm{d}\lambda = \int_{\lambda} I_{\mathrm{PL,ex}}(\lambda) \, \mathrm{d}\lambda + \frac{1}{2} I_{\mathrm{PL,ex}}(\lambda) \, \mathrm{d}\lambda$$

 $\int_{1}^{1} I_{PL,tr}(\lambda) d\lambda$. We observe a gradual evolution of the spectral weight toward trions with increase in the RF input power, as shown in Figure 2c. The results indicate that the ionization rate for excitons is larger than that of trions (see Section 8 in the Supporting Information). Furthermore, we found no variation in the spectral weight, with respect to optical excitation power at RF input power levels of -60 dBm (see Section 9 in the Supporting Information). Hence, we conclude that the observed spectral weight shift in the PL is triggered by the exciton dissociation due to the in-plane electric field component of the traveling SAW field. This results in an increase in the trion formation rate as more free carriers become available, because of the piezoelectric dissociation. 46,47 The conclusion is further supported by the observed increase in the trion binding energy at high RF power, which is strongly correlated to the free carrier density in the system (refer to Section 10 in the Supporting Information). 48,4

We also compare the observed PL quenching in our work with exciton dissociation in other low-dimensional excitonic media, such as GaAs^{33,50} and ZnCdSe⁵¹ quantum wells. Even though almost complete quenching of photoluminescence (PL) under a piezoelectric field has been reported in these works, we do not observe such strong dissociation within our experimental range. This is explained by large exciton binding energy in monolayer semiconductors. This observation also aligns with recent theoretical work by Huang et al.,⁵² where exciton ionization under an electric field in monolayer

semiconductors was shown to be significantly weaker than in the GaAs system.

Stark Shift in Monolayer WSe₂ under Piezoelectric Field. As mentioned earlier, alongside dissociation, the piezoelectric field also triggers PL Stark shift. Spectral redshift of the excitonic energy level due to the electric field of a SAW has been reported for low-dimensional quantum well structures. The excitonic spectral redshift (ΔE) is generally represented by

$$\Delta E = -\frac{1}{2}\alpha E_X^2 \tag{1}$$

where α and E_X refer to the in-plane neutral exciton polarizability and the applied electric field, respectively. The net spectral red shift of the neutral exciton due to piezoelectric field varied with optical incident power (refer to Section 11 in the Supporting Information). Figure 3a shows two Gaussian fittings of monolayer PL spectra at an optical input power of $0.5 \mu W$ under -60 dBm acoustic excitation. Figures 3b and 3c show the red shift of the neutral exciton with the estimated electric field at 0.5 μ W and 4 μ W optical incident power, respectively. The electric field is estimated from the observed PL quenching, as described in Section 12 in the Supporting Information. The error bar represents the spread from PL measurements at four locations on the monolayer. We extract the exciton polarizability by fitting the spectral red shift of the exciton peak with the estimated electric field using eq 1. Based on the experiments at different optical excitation power (see Section 13 in the Supporting Information), we estimate the neutral exciton polarizability in the monolayer to be 8.43 \pm 0.18×10^{-6} Dm/V. We attribute the observed spectral shift to the in-plane electric field of the SAW, since the out-of-plane polarizability of monolayer excitons is smaller by a few orders of magnitude. 12,13 The estimated in-plane polarizability is about an order higher than the reported values in lower dielectric constant environment (hBN)¹¹ and SiO₂.⁵⁶ The observed large in-plane polarizability in this work is due to the strong screening effect from the LiNbO3 substrate that weakens interaction between the bound electron and hole, thereby causing the excitonic state to be more susceptible to the applied electric field. This leads to larger spectral shift in the monolayer PL. 15,16 Generally, it is difficult to verify such an effect due to challenges in fabricating device structures that can apply an in-plane electric field. However, the transfer of monolayer TMD on a piezoelectric substrate, such as that used in this work, offers a simple platform to probe spectral change due to in-plane electric field. We note that the observed spectral redshift cannot be accounted for, because of heating by the surface acoustic wave (please refer to Section 14 in the Supporting Information for detailed discussion). In addition, as discussed in the earlier section, we rule out any possible heating due to optical excitation.

Broadening of Exciton Photoluminescence Line Width under Acoustic Modulation. In low-dimensional semiconductor systems, the broadening of PL can be attributed to various physical mechanisms such as elastic and inelastic scattering with free carriers, phonons, exciton ionization under applied electric field, and dynamic modulation of the bandgap through lattice deformation due to strain. We observe no broadening of the PL spectra with optical input power (see Section 4 in the Supporting Information), and, hence, we rule out broadening due to lattice heating under optical excitation. Alongside, we rule out substrate heating as the dominant

mechanism for spectral modulation, as discussed in the previous section (please refer to Section 14 in the Supporting Information for detailed discussion). Line width broadening due to exciton-free carrier scattering occurs at high excitation densities of >10¹² cm⁻²,⁵⁷ which is 1–2 orders of magnitude higher than the excitation density used in the current experiments. Hence, we assume negligible contribution from scattering with a free carrier. Therefore, we attribute the line width broadening of the exciton PL to dynamic strain³¹ (type-I modulation) in the monolayer and piezoelectric field-induced ionization (type-II modulation).

We estimate the effect of dynamic strain on the exciton spectral line width by calculating the strain tensor,

$$\varepsilon_k = \sum_{i=1}^3 d_{ik} E_i \tag{2}$$

where d is the matrix for the converse piezoelectric effect in the material (128° LiNbO₃ for this work) and E is the piezoelectric field. Based on the strain tensor, we estimate a maximum volumetric strain of ~0.05% at maximum RF input power of 100 mW, using the estimated piezoelectric field in the substrate at acoustic resonance. Finally, we use the strain sensitivity (58 meV/%) of the bandgap of monolayer WSe₂ reported in the literature ^{58,59} and estimate the broadening (Γ_{ε}) due to dynamic strain by the formulation presented in Wei β et al. The estimated volumetric strain and resulting line width broadening of the neutral exciton is shown in Section 15 in the Supporting Information.

We estimate the line width broadening due to piezoelectric field (Γ_{ion}) by following a two-dimensional exciton ionization model. However, to account for strong screening from the surrounding dielectric environment, we use a scaled version of the relationship:

$$\Gamma_{ion}(E) = \beta E_b \sqrt{\frac{\gamma F_0}{F}} \exp\left(-\frac{32}{3} \frac{\gamma F_0}{F}\right)$$
(3)

where β and γ are dimensionless parameters that account for substrate induced dielectric screening that modifies the coulomb interaction in the monolayer. A smaller value of the scaling factor (γ < 1) refers to a stronger screening and hence, a larger line width broadening change under electric field and vice versa. F_0 represents the field required for exciton ionization under substrate induced screening: $F_0 = \frac{E_b^*}{e a_b^*}$; where, E_b^* and a_b^* are the screened exction binding energy and Bohr radius respectively and e is the electronic charge. The total line width broadening under RF excitation can now be written as

$$\Gamma_{RF} - \Gamma_{-60dBm} = \Gamma_{ion}(E) + \Gamma_{\varepsilon}$$

$$= \beta E_b \sqrt{\frac{\gamma F_0}{F}} \exp\left(-\frac{32}{3} \frac{\gamma F_0}{F}\right) + \Gamma_{\varepsilon}$$
(4)

As seen from Figure 4a, the neutral exciton peak broadens with RF power, but the broadening effect decreases as the optical power increases. The results imply that the PL line width broadening is primarily affected by exciton dissociation.

Figure 4b shows the measured line width broadening of the neutral exciton peak and the fitted broadening using eq 4 for an optical input power of 0.5 μ W. We obtain the best fit for β = 9.054 \pm 1.491 and γ = 0.245 \pm 0.009. In contrary to the electric field dependence derived from the simple hydrogen

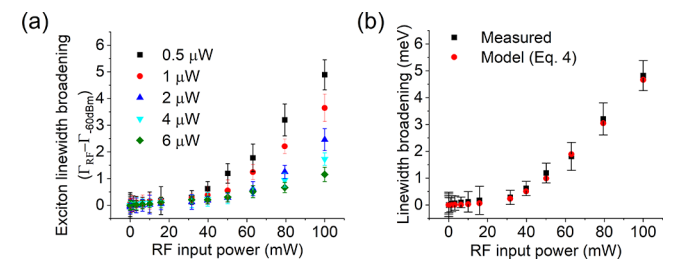


Figure 4. Exciton line width modulation by piezoelectric interaction in monolayer WSe₂. (a) Extracted line width broadening of the exciton peak from PL spectra at different RF input powers. A clear dependence on the free carrier screening process can be observed from the figure. We observe the maximum broadening at the minimum optical power input. (b) Line width broadening fitted as a combined effect of dynamic strain and field induced ionization (as shown in eq 4). The black squares in the figure represent the median of our extracted broadening from PL measurement. The error bars in both plots represents the spread of PL measurements at different positions on the sample.

atom model ($\gamma=1$),⁶⁰ our experimentally measured broadening of the neutral exciton state shows a stronger dependence on the SAW electric field, which is a clear signature of substrate induced screening of coulomb interaction. The strong substrate screening is also observed from the line width broadening at different optical input power (see eq 4 and Section 16 in the Supporting Information). Therefore, we conclude that the observed broadening in the excitonic line width has contributions from both the piezoelectric field (i.e., exciton ionization by the electric field) and dynamic modulation of the monolayer bandgap by the acoustic strain field. The contribution due to the field induced ionization is significantly larger than the strain-induced broadening.

CONCLUSIONS

In conclusion, we have experimentally investigated the interaction of excitons in monolayer WSe2 with the piezoelectric field of a surface acoustic wave. The strong dielectric screening from the LiNbO₃ substrate weakens the coulomb interaction between the electron and hole of the bound excitonic state, thereby increasing the neutral exciton polarizability. Under RF input excitation, the photogenerated excitonic species are readily dissociated via the field-induced ionization. We show that the spectral modulation of the monolayer PL can be controlled by the optically generated free carrier screening. Therefore, the study demonstrates two simultaneous yet independent approaches to control excitonic properties in TMDs. Such control using artificially engineered environmental screening can prove to be extremely beneficial for the realization of next-generation high-speed optoelectronic devices that require rapid and strong dissociation of photogenerated excitonic species.

MATERIALS AND METHODS

Fabrication of SAW Devices on LiNbO_{3μμ}. The SAW devices were fabricated on commercially available 61 128° Y cut LiNbO₃, using standard optical lithography processes. A bilayer photoresist stack (LOR 3A + S1813) was used to ensure good liftoff. LOR 3A was spin-coated at 3000 rpm (thickness ~320 nm), followed by a 5 min baking at 195 °C. Following this, S1813 was spin-coated at 4000 rpm (~1.5 μm). The soft baking of S1813 was performed at 110 °C for 4 min. The samples were exposed using a projection lithography (GCA Autostep AS200) for 0.25 s and developed using AZ-726 MIF (25 s

double puddle recipe). 10-nm Cr and 100-nm Au were evaporated on the samples using electron beam evaporation method. The lift-off was performed by immersing the samples in Microchem Remover PG solution for ~12 h. Following the patterning of the IDTs, a second optical lithography step was performed for patterning the contact pads. For the second step lithography, SPR 220 (3.0) was used as the photoresist (spin speed 2100 rpm). To avoid damage to the IDTs due to the pyroelectric properties of LiNbO3, a low-temperature soft baking method was adopted. The soft baking temperature was gradually ramped up from 65 °C to 85 °C using a hot plate. After 4 min of baking at 85 °C, the temperature was gradually ramped down to 65 °C. The overlay exposure was done using the same projection lithography tool for 0.4 s. Following a delay of 5 min, the exposed samples were developed in AZ-726 MIF (40s double puddle recipe). 10-nm Cr and 500-nm Au were evaporated using electron beam evaporation. The liftoff was performed by immersing the samples in Microchem Remover PG for ~12 h.

Transfer of Monolayer WSe₂ on the Substrate. Monolayer WSe₂ was mechanically exfoliated from a bulk crystal (HQ Graphene) using cellophane tape onto a thin polydimethylsiloxane (PDMS) stamp (GEL-FILM PF-40/1.5-X4) and transferred onto the targeted substrate using a dry transfer technique. 62

Measurement of Acoustic Response. The acoustic response of the SAW devices was measured using a network analyzer (Agilent. Model 4396B) connected to a S-parameter test unit (Agilent, Model 85046A). The S11 response of the SAW devices can be found in the Supporting Information section of the manuscript.

Photoluminescence Measurement under SAW Excitation. Photoluminescence (PL) measurements on the samples were performed using a 450 nm CW laser focused to a diffraction-limited spot. The PL was collected using a 40× 0.95 NA objective (Nikon Plan Apo 40× 0.95) and analyzed using a high-resolution spectrometer (Princeton Instruments IsoPlane SCT 320) coupled to a highly sensitive CCD camera (Princeton Instruments, Model Pixis 400). The PL scans were performed using a high-resolution piezo stage. Transient photoluminescence (TRPL) measurements were done using a 405-nm pulsed laser (Picoquant PDL 800-D), phase locked to the RF excitation source. For TRPL, RF excitation was generated at integer multiple of the laser repetition rate (~5 MHz).

Extraction of Broadening of the Neutral Exciton Peak under RF Excitation. We extract the full width at half-maximum (fwhm) of the neutral exciton peak from the two Gaussian fit of the measured photoluminescence spectrum. We subtract the fwhm at the minimum RF input power used in our work (-60 dBm) from the calculated fwhm at different RF input power to estimate the contribution of different broadening mechanism triggered by the exciton—SAW interaction in the monolayer. In the experiments, an RF input power of -60 dBm is equivalent to RF being OFF, and thus serves as a control for the experiments.

ASSOCIATED CONTENT

Supporting Information

The Supporting Information is available free of charge at https://pubs.acs.org/doi/10.1021/acsnano.1c04269.

Acoustic response of the SAW resonator; calculation of optical fluence and generated exciton density from measured optical power; Gaussian fitting of the PL intensity at 20 dBm RF power; measured monolayer photoluminescence at different optical input power at minimum RF input power at -60 dBm; integrated intensity of measured photoluminescence; integrated intensity of the exciton and trion peaks at -60 dBm RF input excitation at different optical power; PL intensity at $0.5~\mu\text{W}$ and $4~\mu\text{W}$ optical power as a function of RF excitation; dissociation of the overall PL intensity under RF excitation at different optical power; normalized exciton and trion dissociation, with respect to RF input

power; extracted exciton and trion spectral weight from measured photoluminescence at -60 dBm RF input excitation at different optical excitation densities; estimation of increase in trion binding energy for 0.5 μ W optical input power; spectral red shift of the neutral exciton peak due to SAW electric field under optically generated free-carrier screening process; estimation of the electric field and the piezoelectric field; estimation of neutral exciton polarizability at different optical excitation density; monolayer optical response under external heating and consideration of monolayer heating under RF excitation; estimation of line width broadening due to dynamic acoustic strain; fitting of measured exciton line width using dynamic strain and ionization under SAW electric field (PDF)

AUTHOR INFORMATION

Corresponding Author

Parag B. Deotare — Applied Physics Program, University of Michigan, Ann Arbor, Michigan 48109, United States; orcid.org/0000-0002-9867-7380; Phone: 734-647-3119; Email: pdeotare@umich.edu, pdeotare@gmail.com

Authors

Kanak Datta — Electrical Engineering and Computer Science, University of Michigan, Ann Arbor, Michigan 48109, United States; orcid.org/0000-0003-4086-3225

Zidong Li — Electrical Engineering and Computer Science, University of Michigan, Ann Arbor, Michigan 48109, United States; oocid.org/0000-0002-0984-9778

Zhengyang Lyu – Applied Physics Program, University of Michigan, Ann Arbor, Michigan 48109, United States

Complete contact information is available at: https://pubs.acs.org/10.1021/acsnano.1c04269

Funding

P.B.D. acknowledges partial support of this work by the Air Force Office of Scientific Research (AFOSR), Award No. FA9550-17-1-0208 and the National Science Foundation (NSF) (Grant No. DMR-1904541).

Notes

The authors declare no competing financial interest.

ACKNOWLEDGMENTS

The authors would like to thank the Lurie Nanofabrication Facility at the University of Michigan, Ann Arbor where the device fabrication was performed. The authors would like to thank Arun Nagpal and Darwin Cordovilla for their help and fruitful discussions.

REFERENCES

- (1) Manzeli, S.; Ovchinnikov, D.; Pasquier, D.; Yazyev, O. V.; Kis, A. 2D Transition Metal Dichalcogenides. *Nat. Rev. Mater.* **2017**, *2*, 1–15.
- (2) Jariwala, D.; Sangwan, V. K.; Lauhon, L. J.; Marks, T. J.; Hersam, M. C. Emerging Device Applications for Semiconducting Two-Dimensional Transition Metal Dichalcogenides. *ACS Nano* **2014**, 8 (2), 1102–1120.
- (3) Schneider, C.; Glazov, M. M.; Korn, T.; Höfling, S.; Urbaszek, B. Two-Dimensional Semiconductors in the Regime of Strong Light-Matter Coupling. *Nat. Commun.* **2018**, *9* (1), 1–9.
- (4) Chernikov, A.; Berkelbach, T. C.; Hill, H. M.; Rigosi, A.; Li, Y.; Aslan, O. B.; Reichman, D. R.; Hybertsen, M. S.; Heinz, T. F. Exciton

- Binding Energy and Nonhydrogenic Rydberg Series in Monolayer WS₂. Phys. Rev. Lett. **2014**, 113 (7), 076802.
- (5) Ross, J. S.; Klement, P.; Jones, A. M.; Ghimire, N. J.; Yan, J.; Mandrus, D. G.; Taniguchi, T.; Watanabe, K.; Kitamura, K.; Yao, W.; Cobden, D. H.; Xu, X. Electrically Tunable Excitonic Light-Emitting Diodes Based on Monolayer WSe₂ p—n Junctions. *Nat. Nanotechnol.* **2014**, *9* (4), 268–272.
- (6) Baugher, B. W. H.; Churchill, H. O. H.; Yang, Y.; Jarillo-Herrero, P. Optoelectronic Devices Based on Electrically Tunable *p-n* Diodes in a Monolayer Dichalcogenide. *Nat. Nanotechnol.* **2014**, 9 (4), 262–267
- (7) Weiß, M.; Krenner, H. J. Interfacing Quantum Emitters with Propagating Surface Acoustic Waves. J. Phys. D: Appl. Phys. 2018, 51 (37), 373001.
- (8) Delsing, P.; Cleland, A. N.; Schuetz, M. J. A.; Knörzer, J.; Giedke, G.; Cirac, J. I.; Srinivasan, K.; Wu, M.; Balram, K. C.; Baüerle, C.; Meunier, T.; Ford, C. J. B.; Santos, P. V.; Cerda-Méndez, E.; Wang, H.; Krenner, H. J.; Nysten, E. D. S.; Weiß, M.; Nash, G. R.; Thevenard, L.; et al. The 2019 Surface Acoustic Waves Roadmap. J. Phys. D. Appl. Phys. 2019, 52 (35), 353001.
- (9) Sogawa, T.; Sanada, H.; Gotoh, H.; Yamaguchi, H.; Santos, P. V. Dynamic Control of Photoluminescence Polarization Properties in GaAs/AlAs Quantum Wells by Surface Acoustic Waves. *Phys. Rev. B: Condens. Matter Mater. Phys.* **2012**, *86* (3), 035311.
- (10) Alsina, F.; Santos, P. V.; Hey, R.; García-Cristóbal, A.; Cantarero, A. Dynamic Carrier Distribution in Quantum Wells Modulated by Surface Acoustic Waves. *Phys. Rev. B: Condens. Matter Mater. Phys.* **2001**, *64* (4), 1–4.
- (11) Kinzel, J. B.; Rudolph, D.; Bichler, M.; Abstreiter, G.; Finley, J. J.; Koblmüller, G.; Wixforth, A.; Krenner, H. J. Directional and Dynamic Modulation of the Optical Emission of an Individual GaAs Nanowire Using Surface Acoustic Waves. *Nano Lett.* **2011**, *11* (4), 1512–1517.
- (12) Hernández-Mínguez, A.; Möller, M.; Breuer, S.; Pfüller, C.; Somaschini, C.; Lazić, S.; Brandt, O.; García-Cristóbal, A.; De Lima, M. M.; Cantarero, A.; Geelhaar, L.; Riechert, H.; Santos, P. V. Acoustically Driven Photon Antibunching in Nanowires. *Nano Lett.* **2012**, *12* (1), 252–258.
- (13) Lazić, S.; Chernysheva, E.; Gačević; Van Der Meulen, H. P.; Calleja, E.; Calleja Pardo, J. M. Dynamic Control of the Optical Emission from GaN/InGaN Nanowire Quantum Dots by Surface Acoustic Waves. *AIP Adv.* **2015**, *5* (9), 97217.
- (14) Pustiowski, J.; Müller, K.; Bichler, M.; Koblmüller, G.; Finley, J. J.; Wixforth, A.; Krenner, H. J. Independent Dynamic Acousto-Mechanical and Electrostatic Control of Individual Quantum Dots in a LiNbO₃-GaAs Hybrid. *Appl. Phys. Lett.* **2015**, *106* (1), 13107.
- (15) Rezk, A. R.; Carey, B.; Chrimes, A. F.; Lau, D. W. M.; Gibson, B. C.; Zheng, C.; Fuhrer, M. S.; Yeo, L. Y.; Kalantar-Zadeh, K. Acoustically-Driven Trion and Exciton Modulation in Piezoelectric Two-Dimensional MoS₂. *Nano Lett.* **2016**, *16* (2), 849–855.
- (16) Rezk, A. R.; Walia, S.; Ramanathan, R.; Nili, H.; Ou, J. Z.; Bansal, V.; Friend, J. R.; Bhaskaran, M.; Yeo, L. Y.; Sriram, S. Acoustic-Excitonic Coupling for Dynamic Photoluminescence Manipulation of Quasi-2D MoS₂ Nanoflakes. *Adv. Opt. Mater.* **2015**, 3 (7), 888–894.
- (17) Lazić, S.; Espinha, A.; Pinilla Yanguas, S.; Gibaja, C.; Zamora, F.; Ares, P.; Chhowalla, M.; Paz, W. S.; Burgos, J. J. P.; Hernández-Mínguez, A.; Santos, P. V.; van der Meulen, H. P. Dynamically Tuned Non-Classical Light Emission from Atomic Defects in Hexagonal Boron Nitride. *Commun. Phys.* **2019**, 2 (1), 1–8.
- (18) Preciado, E.; Schülein, F. J. R.; Nguyen, A. E.; Barroso, D.; Isarraraz, M.; Von Son, G.; Lu, I. H.; Michailow, W.; Möller, B.; Klee, V.; Mann, J.; Wixforth, A.; Bartels, L.; Krenner, H. J. Scalable Fabrication of a Hybrid Field-Effect and Acousto-Electric Device by Direct Growth of Monolayer MoS₂/LiNbO₃. *Nat. Commun.* **2015**, *6* (1), 1–8.
- (19) Zheng, S.; Wu, E.; Feng, Z.; Zhang, R.; Xie, Y.; Yu, Y.; Zhang, R.; Li, Q.; Liu, J.; Pang, W.; Zhang, H.; Zhang, D. Acoustically Enhanced Photodetection by a Black Phosphorus-MoS₂ van der

- Waals Heterojunction *p-n* Diode. *Nanoscale* **2018**, *10* (21), 10148–10153.
- (20) Bandhu, L.; Lawton, L. M.; Nash, G. R. Macroscopic Acoustoelectric Charge Transport in Graphene. *Appl. Phys. Lett.* **2013**, *103* (13), 133101.
- (21) Miseikis, V.; Cunningham, J. E.; Saeed, K.; O'Rorke, R.; Davies, A. G. Acoustically Induced Current Flow in Graphene. *Appl. Phys. Lett.* **2012**, *100* (13), 133105.
- (22) Zheng, S.; Zhang, H.; Feng, Z.; Yu, Y.; Zhang, R.; Sun, C.; Liu, J.; Duan, X.; Pang, W.; Zhang, D. Acoustic Charge Transport Induced by the Surface Acoustic Wave in Chemical Doped Graphene. *Appl. Phys. Lett.* **2016**, *109* (18), 183110.
- (23) Poole, T.; Nash, G. R. Acoustoelectric Current in Graphene Nanoribbons. *Sci. Rep.* **2017**, *7* (1), 1–9.
- (24) Yokoi, M.; Fujiwara, S.; Kawamura, T.; Arakawa, T.; Aoyama, K.; Fukuyama, H.; Kobayashi, K.; Niimi, Y. Negative Resistance State in Superconducting NbSe₂ Induced by Surface Acoustic Waves. *Sci. Adv.* **2020**, *6* (34), No. eaba1377.
- (25) Cavalcante, L. S. R.; Da Costa, D. R.; Farias, G. A.; Reichman, D. R.; Chaves, A. Stark Shift of Excitons and Trions in Two-Dimensional Materials. *Phys. Rev. B: Condens. Matter Mater. Phys.* **2018**, 98 (24), 245309.
- (26) Pedersen, T. G. Exciton Stark Shift and Electroabsorption in Monolayer Transition-Metal Dichalcogenides. *Phys. Rev. B: Condens. Matter Mater. Phys.* **2016**, 94 (12), 125424.
- (27) Massicotte, M.; Vialla, F.; Schmidt, P.; Lundeberg, M. B.; Latini, S.; Haastrup, S.; Danovich, M.; Davydovskaya, D.; Watanabe, K.; Taniguchi, T.; Fal'ko, V. I.; Thygesen, K. S.; Pedersen, T. G.; Koppens, F. H. L. Dissociation of Two-Dimensional Excitons in Monolayer WSe₂. *Nat. Commun.* **2018**, *9* (1), 1–7.
- (28) Klein, J.; Wierzbowski, J.; Regler, A.; Becker, J.; Heimbach, F.; Müller, K.; Kaniber, M.; Finley, J. J. Stark Effect Spectroscopy of Mono- and Few-Layer MoS₂. *Nano Lett.* **2016**, *16* (3), 1554–1559.
- (29) Roch, J. G.; Leisgang, N.; Froehlicher, G.; Makk, P.; Watanabe, K.; Taniguchi, T.; Schönenberger, C.; Warburton, R. J. Quantum-Confined Stark Effect in a MoS₂ Monolayer van der Waals Heterostructure. *Nano Lett.* **2018**, *18* (2), 1070–1074.
- (30) Verzhbitskiy, I.; Vella, D.; Watanabe, K.; Taniguchi, T.; Eda, G. Suppressed Out-of-Plane Polarizability of Free Excitons in Monolayer WSe₂. ACS Nano **2019**, 13 (3), 3218–3224.
- (31) Violante, A.; Cohen, K.; Lazić, S.; Hey, R.; Rapaport, R.; Santos, P. V. Dynamics of Indirect Exciton Transport by Moving Acoustic Fields. *New J. Phys.* **2014**, *16* (3), 033035.
- (32) Rudolph, J.; Hey, R.; Santos, P. V. Long-Range Exciton Transport by Dynamic Strain Fields in a GaAs Quantum Well. *Phys. Rev. Lett.* **2007**, 99 (4), 1–4.
- (33) Rocke, C.; Zimmermann, S.; Wixforth, A.; Kotthaus, J. P.; Böhm, G.; Weimann, G. Acoustically Driven Storage of Light in a Quantum Well. *Phys. Rev. Lett.* **1997**, 78 (21), 4099–4102.
- (34) Morgan, D. Surface Acoustic Wave Filters; Elsevier, Ltd., Burlington, MA, 2007, DOI: 10.1016/B978-0-12-372537-0.X5000-6. (35) Komsa, H. P.; Krasheninnikov, A. V. Effects of Confinement and Environment on the Electronic Structure and Exciton Binding Energy of MoS₂ from First Principles. Phys. Rev. B: Condens. Matter Mater. Phys. 2012, 86 (24), 241201.
- (36) Berkelbach, T. C.; Hybertsen, M. S.; Reichman, D. R. Theory of Neutral and Charged Excitons in Monolayer Transition Metal Dichalcogenides. *Phys. Rev. B: Condens. Matter Mater. Phys.* **2013**, 88 (4), 045318.
- (37) Lin, Y.; Ling, X.; Yu, L.; Huang, S.; Hsu, A. L.; Lee, Y. H.; Kong, J.; Dresselhaus, M. S.; Palacios, T. Dielectric Screening of Excitons and Trions in Single-Layer MoS₂. *Nano Lett.* **2014**, *14* (10), 5569–5576.
- (38) Stier, A. V.; Wilson, N. P.; Clark, G.; Xu, X.; Crooker, S. A. Probing the Influence of Dielectric Environment on Excitons in Monolayer WSe₂: Insight from High Magnetic Fields. *Nano Lett.* **2016**, *16* (11), 7054–7060.
- (39) Aivazian, G.; Gong, Z.; Jones, A. M.; Chu, R. L.; Yan, J.; Mandrus, D. G.; Zhang, C.; Cobden, D.; Yao, W.; Xu, X. Magnetic

- Control of Valley Pseudospin in Monolayer WSe 2. Nat. Phys. 2015, 11 (2), 148-152.
- (40) Arora, A.; Koperski, M.; Nogajewski, K.; Marcus, J.; Faugeras, C.; Potemski, M. Excitonic Resonances in Thin Films of WSe₂: From Monolayer to Bulk Material. *Nanoscale* **2015**, 7 (23), 10421–10429. (41) Huang, J.; Hoang, T. B.; Mikkelsen, M. H. Probing the Origin
- of Excitonic States in Monolayer WSe₂. Sci. Rep. **2016**, 6 (1), 1–7.
- (42) You, Y.; Zhang, X. X.; Berkelbach, T. C.; Hybertsen, M. S.; Reichman, D. R.; Heinz, T. F. Observation of Biexcitons in Monolayer WSe₂. *Nat. Phys.* **2015**, *11* (6), 477–481.
- (43) He, M.; Rivera, P.; Van Tuan, D.; Wilson, N. P.; Yang, M.; Taniguchi, T.; Watanabe, K.; Yan, J.; Mandrus, D. G.; Yu, H.; Dery, H.; Yao, W.; Xu, X. Valley Phonons and Exciton Complexes in a Monolayer Semiconductor. *Nat. Commun.* **2020**, *11* (1), 1–7.
- (44) Rivera, P.; He, M.; Kim, B.; Liu, S.; Rubio-Verdú, C.; Moon, H.; Mennel, L.; Rhodes, D. A.; Yu, H.; Taniguchi, T.; Watanabe, K.; Yan, J.; Mandrus, D. G.; Dery, H.; Pasupathy, A.; Englund, D.; Hone, J.; Yao, W.; Xu, X. Intrinsic Donor-Bound Excitons in Ultraclean Monolayer Semiconductors. *Nat. Commun.* 2021, 12 (1), 1–8.
- (45) Wei, K.; Liu, Y.; Yang, H.; Cheng, X.; Jiang, T. Large Range Modification of Exciton Species in Monolayer WS₂. *Appl. Opt.* **2016**, 55 (23), 6251.
- (46) Mouri, S.; Miyauchi, Y.; Matsuda, K. Tunable Photoluminescence of Monolayer MoS₂ via Chemical Doping. Nano Lett. **2013**, 13 (12), 5944–5948.
- (47) Singh, A.; Moody, G.; Tran, K.; Scott, M. E.; Overbeck, V.; Berghäuser, G.; Schaibley, J.; Seifert, E. J.; Pleskot, D.; Gabor, N. M.; Yan, J.; Mandrus, D. G.; Richter, M.; Malic, E.; Xu, X.; Li, X. Trion Formation Dynamics in Monolayer Transition Metal Dichalcogenides. *Phys. Rev. B: Condens. Matter Mater. Phys.* **2016**, 93 (4), 041401.
- (48) Siviniant, J.; Scalbert, D.; Kavokin, A. V.; Coquillat, D.; Lascaray, J. P. Chemical Equilibrium between Excitons, Electrons, and Negatively Charged Excitons in Semiconductor Quantum Wells. *Phys. Rev. B: Condens. Matter Mater. Phys.* 1999, 59 (3), 1602–1604.
- (49) Kheng, K.; Cox, R. T.; D'Aubigné, M. Y.; Bassani, F.; Saminadayar, K.; Tatarenko, S. Observation of Negatively Charged Excitons X- in Semiconductor Quantum Wells. *Phys. Rev. Lett.* **1993**, 71 (11), 1752–1755.
- (50) Santos, P. V.; Ramsteiner, M.; Jungnickel, F. Spatially Resolved Photoluminescence in GaAs Surface Acoustic Wave Structures. *Appl. Phys. Lett.* **1998**, 72 (17), 2099–2101.
- (51) Fuhrmann, D. A.; Wixforth, A.; Curran, A.; Morrod, J. K.; Prior, K. A.; Warburton, R. J.; Ebbecke, J. Surface Acoustic Wave Mediated Exciton Dissociation in a ZnCdSe/ LiNbO₃ Hybrid. *Appl. Phys. Lett.* **2009**, *94* (19), 193505.
- (52) Huang, T.; Han, P.; Wang, X.; Ye, J.; Sun, W.; Feng, S.; Zhang, Y. Theoretical Study on Dynamic Acoustic Modulation of Free Carriers, Excitons, and Trions in 2D MoS₂ Flake. *J. Phys. D: Appl. Phys.* **2017**, *50* (11), 114005.
- (53) Santos, P. V.; Alsina, F.; Stotz, J. A. H.; Hey, R.; Eshlaghi, S.; Wieck, A. D. Band Mixing and Ambipolar Transport by Surface Acoustic Waves in GaAs Quantum Wells. *Phys. Rev. B: Condens. Matter Mater. Phys.* **2004**, *69* (15), 155318.
- (54) Ivanov, A. L.; Littlewood, P. B. Acoustically Induced Stark Effect for Excitons in Intrinsic Semiconductors. *Phys. Rev. Lett.* **2001**, 87 (13), 136403.
- (55) Choy, W. C. H.; Li, E. H.; Weiss, B. L. Electro-Optic and Electro-Absorptive Modulations of AlGaAs/GaAs Quantum Well Using Surface Acoustic Wave. J. Appl. Phys. 1998, 83 (2), 858–866.
- (56) Sun, Z.; Beaumariage, J.; Xu, K.; Liang, J.; Hou, S.; Forrest, S. R.; Fullerton-Shirey, S. K.; Snoke, D. W. Electric-Field-Induced Optical Hysteresis in Single-Layer WSe₂. *Appl. Phys. Lett.* **2019**, *115* (16), 161103.
- (57) Chernikov, A.; Van Der Zande, A. M.; Hill, H. M.; Rigosi, A. F.; Velauthapillai, A.; Hone, J.; Heinz, T. F. Electrical Tuning of Exciton Binding Energies in Monolayer WS₂. *Phys. Rev. Lett.* **2015**, *115* (12), 126802.

- (58) Schmidt, R.; Niehues, I.; Schneider, R.; Drüppel, M.; Deilmann, T.; Rohlfing, M.; De Vasconcellos, S. M.; Castellanos-Gomez, A.; Bratschitsch, R. Reversible Uniaxial Strain Tuning in Atomically Thin WSe₂. 2D Mater. **2016**, 3 (2), 021011.
- (59) Aas, S.; Bulutay, C. Strain Dependence of Photoluminescence and Circular Dichroism in Transition Metal Dichalcogenides: A k · p Analysis. *Opt. Express* **2018**, *26* (22), 28672.
- (60) Miller, D. A. B.; Chemla, D. S.; Damen, T. C.; Gossard, A. C.; Wiegmann, W.; Wood, T. H.; Burrus, C. A. Electric Field Dependence of Optical Absorption near the Band Gap of Quantum-Well Structures. *Phys. Rev. B: Condens. Matter Mater. Phys.* 1985, 32 (2), 1043–1060.
- (61) Lithium Niobate wafers; available via the Internet at: http://www.pmoptics.com/LiNbO3.html (accessed Feb. 13, 2021).
- (62) Castellanos-Gomez, A.; Buscema, M.; Molenaar, R.; Singh, V.; Janssen, L.; Van Der Zant, H. S. J.; Steele, G. A. Deterministic Transfer of Two-Dimensional Materials by All-Dry Viscoelastic Stamping. 2D Mater. 2014, 1 (1), 011002.